Journal of The Electrochemical Society, **155** (1) H43-H46 (2008)
0013-4651/2007/155(1)/H43/4/$23.00 © The Electrochemical Society

Physical and Electrical Properties of Atomic-Layer-Deposited $Hf_xZr_{1-x}O_2$ with TEMAHf, TEMAZr, and Ozone

D. H. Triyoso,[a,z] R. Gregory, M. Park,[b] K. Wang,[b] and S. I. Lee[b]

[a]*Freescale Semiconductor, Incorporated, Technology Solutions Organization, Austin, Texas 78721, USA*
[b]*Vesta Technology, San Jose, California 95134, USA*

In this work, physical and electrical characteristics of atomic-layer-deposited $Hf_xZr_{1-x}O_2$ formed using tetrakis-ethylmethylaminohafnium (TEMAHf), tetrakis-ethylmethylaminozirconium (TEMAZr), and ozone are reported. Confirming Zr addition, film densities decrease with increasing Zr content. A slight increase in interfacial layer thickness is observed for ZrO_2 after high-temperature annealing. All films remain smooth and void-free after high-temperature annealing. Tetragonal phase stabilization is observed with increasing Zr content. Carbon impurities are low and independent of Zr content. $Hf_xZr_{1-x}O_2$ transistors and capacitors are fabricated for electrical characterization. Well-behaved capacitance–voltage characteristics are observed for all devices. Only a slight increase in gate leakage current is observed as Zr content is increased from $<2\%$ (HfO_2) to $\sim 50\%$ ($Hf_{0.5}Zr_{0.5}O_2$). $Hf_xZr_{1-x}O_2$ devices have ~ 50 mV lower threshold voltage than HfO_2 devices. High field mobilities of $Hf_xZr_{1-x}O_2$ devices with 50 and 60% Zr content are higher than HfO_2 or ZrO_2. All these results indicate $Hf_xZr_{1-x}O_2$ is a promising dielectric for SiO_2 replacement.
 [DOI: 10.1149/1.2803427]

Manuscript submitted August 6, 2007; revised manuscript received September 25, 2007.
Available electronically November 9, 2007.

The semiconductor industry has expended much effort to find a suitable high-*k* material to replace SiON gate dielectrics. In the past few years hafnium-based high-*k* dielectrics have been identified as promising materials for SiON replacement due to their excellent thermal stabilities with Si substrate and their high dielectric constants. However, as HfO_2 thickness is reduced, the *k*-value decreases to <15. Furthermore, HfO_2 suffers from mobility degradation, fixed charge issues, threshold voltage instability, and a *k* variation dependence on crystal structure. We have recently reported that Zr addition into HfO_2 leads to improved HfO_2 reliability, mobility, and scalability.[1-4] $Hf_xZr_{1-x}O_2$ transistors with excellent electrical characteristics have recently been fabricated.[1-4]

Among the various methods available to deposit thin high-*k* films, atomic layer deposition (ALD) is considered the most promising due to its precise thickness control, easy composition control, excellent conformality, and low deposition temperature. ALD is a chemical gas-phase self-limiting deposition based on alternative saturative surface reactions. In ALD the chemical precursors are alternately pulsed into the reactor where surface reactions occur. More details on the chemistry of ALD and various applications of ALD have recently been reviewed.[5,6] Many chemical precursors have been investigated for ALD Hf-based dielectrics such as halide-based precursors and metallorganic precursors. Tetrakis-ethylmethylaminohafnium (TEMAHf) has been one of the most popular choices for ALD Hf metal precursor because it results in a film with few impurities,[7,8] adequate deposition rate, and good electrical properties.[9] In this paper we report physical and electrical characteristics of $Hf_xZr_{1-x}O_2$ high-*k* gate dielectrics fabricated using TEMAHf, tetrakis-ethylmethylaminozirconium (TEMAZr), and ozone. Detailed physical properties of $Hf_xZr_{1-x}O_2$ as a function of Zr content were studied using X-ray reflectivity (XRR), atomic force microscopy (AFM), X-ray diffraction (XRD), and secondary ion mass spectrometry (SIMS). Electrical properties were investigated by fabricating $Hf_xZr_{1-x}O_2$ transistors and capacitors.

Experimental

ALD $Hf_xZr_{1-x}O_2$ films ($x = 0$, 0.25, 0.4, 0.5, and 1) were fabricated at 330°C wafer temperature using TEMAHf, TEMAZr, and O_3. The dielectric layer was grown on a chemical oxide starting surface. The chemical oxide was formed by cleaning Si wafers in a solution of deionized water, hydrogen peroxide, and hydrochloric acid. The wafers were immersed in this solution for 10 min at 35°C. Unless indicated otherwise, films were annealed at 1000°C for 5 s in N_2 with a 70 Å TiN capping layer in place. The capping layer was removed using a conventional wet-etch selective to TiN prior to physical characterization. Recent work shows the benefit of using a capping layer to prevent void formation and to stabilize the tetragonal phase in HfO_2.[10] XRD, performed with Cu Kα radiation from a Rigaku Rotaflex RU-200BH rotating anode system, was used to investigate the microstructure of the films. Film density was measured using Jordan Valley X-ray reflectometry (XRR). XRR measurements utilize glancing-angle X-rays with wavelength on the order of 1 Å to probe the film. The X-rays incident below the critical angle are totally reflected. Beyond the critical angle, X-rays penetrate the film, which results in reflected interference patterns. The resultant interference spectra provides thickness, density, and surface and interface roughness. Film roughness was measured by AFM operated in tapping mode. The root-mean-square (rms) roughness values were calculated on 1×1 μm images. SIMS was performed with a primary Cs^+ beam at 2 keV and 60° for detecting secondary ions of C and Si. To extract work-function and dielectric fixed charge, wafers were prepared with varying thicknesses of SiO_2. The SiO_2 thickness series was formed by growing 100 Å of thermal SiO_2 and then using a spin etcher with 20:1 ratio of water to hydrofluoric (HF) acid to etch concentric rings into the SiO_2. This process produces a wafer with three tiers of SiO_2 thicknesses (0, 50, and 100 Å) called a "cake SiO_2" wafer. Every wafer prepared in this fashion received ~ 30 Å of ALD $Hf_xZr_{1-x}O_2$ high-*k* dielectric followed by 100 Å physical vapor deposited (PVD) TaC_y metal gate electrode. These HfO_2/TaC_y gate stacks were then capped with poly-Si. High-*k* devices were fabricated with this gate stack using conventional complementary metal oxide semiconductor (CMOS) integration with sidewall liners and spacers, implants to the Si-cap/source/drain, 1000°C activation anneal, co-salicide contacts, and forming gas anneal. The work-function extraction was performed on 80×80 μm capacitor structures, as previously reported.[11,12] Capacitance-voltage (*C-V*) and current-voltage (*I-V*) measurements were also performed on 80×85 μm capacitor structures. Cyclic voltammograms (CVs) were measured at 100 kHz.

Results and Discussion

Figure 1a plots XRR density of ~ 25 Å $Hf_xZr_{1-x}O_2$ with varying Zr content for as-deposited and annealed films. Results show that in general, film density decreases as Zr content is increased. This is expected as ZrO_2 (5.85 g/cm^3) has a lower density than HfO_2 (9.68 g/cm^3). The density values are reasonably close to bulk values. There is no significant difference in film density between as-

[z] E-mail: dina.triyoso@freescale.com

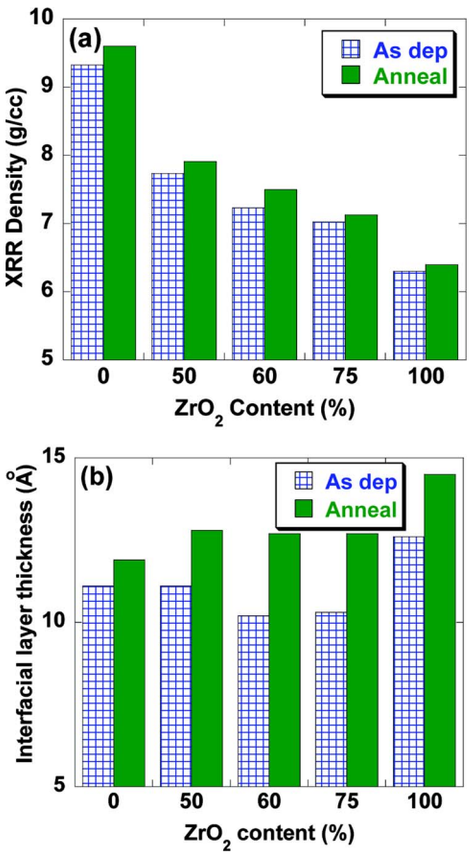

Figure 1. (Color online) (a) XRR density and interfacial layer thickness for as-deposited and annealed ~25 Å $Hf_xZr_{1-x}O_2$ (x = 0–1) films. Films are annealed at 1000°C in a nitrogen ambient with a capping layer in place. The capping layer was removed prior to XRR measurement.

deposited and annealed films. The thickness of the interfacial layer between the high-k and Si is estimated from the difference in thickness values obtained by ellipsometry and XRR measurement as previously reported.[13] Figure 1b compares the thickness of interfacial layers for as-deposited and annealed films. For as-deposited films, interfacial layer thicknesses increase slightly from ~10 to 11 Å for HfO_2 and $Hf_xZr_{1-x}O_2$ (x = 0.25–0.75) to 12.6 Å for ZrO_2. The same trend is also observed for annealed films. Interfacial layer thickness increases from ~12 to 14.5 Å. Comparing film density for a fixed composition, it is apparent that an increase in density is observed after annealing in a nitrogen ambient at 1000°C for all films studied. The smallest and largest increase in interfacial layer induced by annealing is observed for HfO_2 (~1 Å) and ZrO_2 (~2 Å), respectively. This increase in interfacial layer thickness for annealed ZrO_2 is not observed for ZrO_2 formed by metal halide and water as precursors.[14] The fact that ozone is an oxidizer stronger than water may play a role in this increase in interfacial layer thickness.

To study film morphology, AFM images were taken for ~25 Å films after high-temperature annealing and are shown in Fig. 2. All $Hf_xZr_{1-x}O_2$ films remain smooth and void-free, regardless of Zr content. The roughness values of these films (~0.18 to 0.19 nm) are comparable to their as-deposited values and to films deposited using $HfCl_4/ZrCl_4$. To study film microstructure, XRD spectra for ~250 Å $Hf_xZr_{1-x}O_2$ films were acquired and are plotted in Fig. 3. XRD spectra show HfO_2 to be predominantly monoclinic. It is noted that HfO_2 deposited using halide precursor is a mixture of monoclinic and tetragonal phases instead of mostly monoclinic phase, as seen in HfO_2 deposited using TEMAHf and TEMAZr. This difference suggests that the choice of precursors can have subtle impact

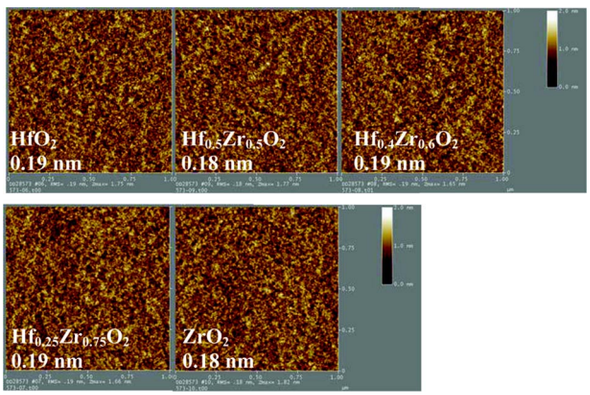

Figure 2. (Color online) AFM images for ~25 Å $Hf_xZr_{1-x}O_2$ (x = 0, 0.25, 0.4, 0.5, or 1) films. Image size is 1 × 1 μm. The rms values are included on the images. All films are annealed at 1000°C in a nitrogen ambient with a capping layer in place. The capping layer was removed prior to AFM analysis.

on film microstructure. As Zr is added, films become a mixture of monoclinic and tetragonal phases. With pure ZrO_2, films become predominantly tetragonal. This microstructure study highlights the stabilization of tetragonal phase with Zr addition. This tetragonal phase stabilization is also observed with $Hf_xZr_{1-x}O_2$ deposited using $HfCl_4$ and $ZrCl_4$.[3,14] The phase diagram of the HfO_2–ZrO_2 system indicates that (*i*) the monoclinic phase is the equilibrium phase across the compositional range and (*ii*) ZrO_2 polymorphs have lower transition temperatures than the HfO_2 polymorphs. Therefore, at 1000°C anneal temperature the free energy difference in driving the tetragonal-to-monoclinic or amorphous-to-monoclinic phase transformation is reduced as an increasing amount of ZrO_2 is alloyed into $Hf_xZr_{1-x}O_2$. Film impurities are investigated with SIMS. SIMS carbon depth profiles for ~250 Å $Hf_xZr_{1-x}O_2$ films are shown in Fig. 4. Carbon impurities are low for all Zr concentrations examined. ZrO_2 has slightly higher carbon impurity than the other films examined. Carbon depth profiles for all films examined appear to be fairly uniform throughout the bulks of the films.

To investigate electrical characteristics, $Hf_xZr_{1-x}O_2$ transistors and capacitors were fabricated with TaC_y metal gates. Well-behaved C-V characteristics were obtained for all $Hf_xZr_{1-x}O_2$ devices. The C-V curves are plotted in Fig. 5a. Equivalent oxide thicknesses (EOTs) for films with 0, 50, 60, 75, and 100% ZrO_2 content are 11.3, 11.5, 11.6, 11.7, and 11.5 Å, respectively. We believe that as Zr content is increased, the k value increase due to tetragonal phase

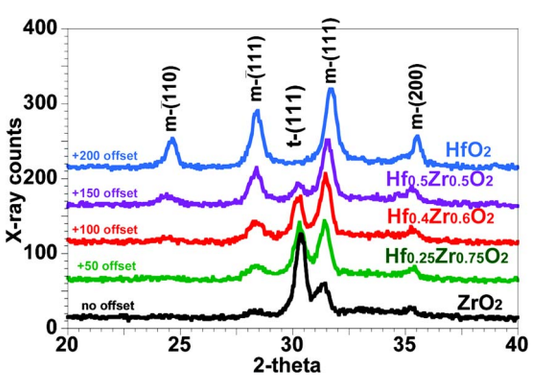

Figure 3. (Color online) XRD spectra for ~250 Å $Hf_xZr_{1-x}O_2$ (x = 0, 0.25, 0.4, 0.5, or 1) films. All films are annealed at 1000°C in a nitrogen ambient with a capping layer in place. The capping layer was removed prior to XRD analysis.

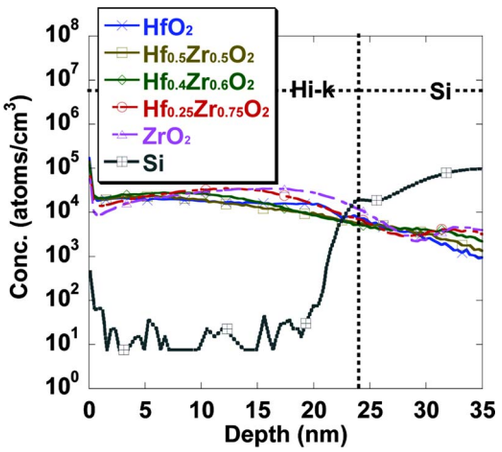

Figure 4. (Color online) SIMS carbon depth profiles for ~250 Å $Hf_xZr_{1-x}O_2$ (x = 0, 0.25, 0.4, 0.5, or 1) films. All films are annealed at 1000°C in a nitrogen ambient with a capping layer in place. The capping layer was removed prior to SIMS analysis.

stabilization is offset by the increase in interfacial layer thickness (see Fig. 1b). That is why we do not see a reduction in overall EOT as a result of Zr addition. Gate leakage current characteristics for $Hf_xZr_{1-x}O_2$ devices are shown in Fig. 5b. Some increase in leakage current with Zr addition is expected, as ZrO_2 has a smaller bandgap than HfO_2.[14] A slight increase in leakage current at the high-applied-voltage region is observed as Zr content is increased from <2% (HfO_2) to ~50% ($Hf_{0.5}Zr_{0.5}O_2$). No significant increase in leakage

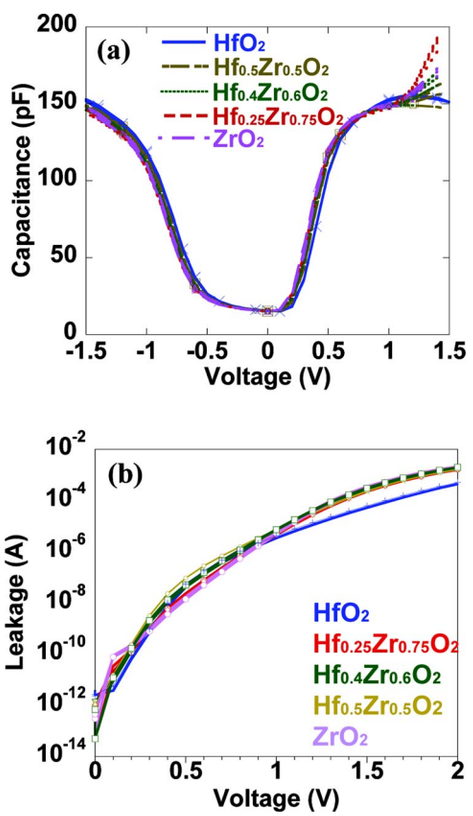

Figure 5. (Color online) (a) *C-V* and (b) gate leakage–current voltage for ~25 Å $Hf_xZr_{1-x}O_2$ (x = 0, 0.25, 0.4, 0.5, or 1) devices. Device size is 85 × 80 μm.

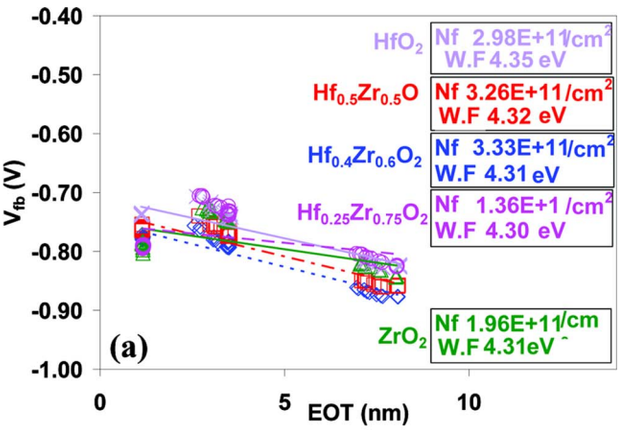

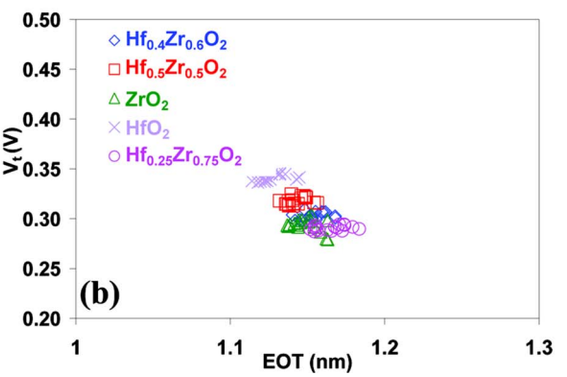

Figure 6. (Color online) Plots of (a) V_{FB} vs EOT and (b) V_t vs EOT for ~25 Å $Hf_xZr_{1-x}O_2$ (x = 0, 0.25, 0.4, 0.5, or 1) devices. Device size is 85 × 80 μm.

current is observed as Zr content is further increased from 50% ($Hf_{0.5}Zr_{0.5}O_2$) to 100% (ZrO_2). Figure 6a plots flatband voltage (V_{FB}) vs EOT for $Hf_xZr_{1-x}O_2$ devices from which work-function and fixed charge values are extracted. The work function of a $Hf_xZr_{1-x}O_2$ device with TaC_y metal gate is determined to be ~4.3 eV. The work function is unchanged with increasing Zr content. Fixed charge in $Hf_xZr_{1-x}O_2$ measures ~10^{11} cm^{-2} for all devices with varying Zr content. Figure 6b shows a plot of (threshold voltage) V_t vs EOT for $Hf_xZr_{1-x}O_2$ devices. $Hf_xZr_{1-x}O_2$ devices (x = 0.5–1.0) have ~50 mV lower V_t values than HfO_2 devices. Figure 7 shows high field mobility relative to universal mobility for $Hf_xZr_{1-x}O_2$ devices. Results show $Hf_xZr_{1-x}O_2$ devices with 50–60% Zr content have the best mobility compared to HfO_2 and ZrO_2. Note also that the ZrO_2 devices have more scatter in mobility than $Hf_xZr_{1-x}O_2$ devices. We believe that the improvement in high-field mobility is related to a higher quality of interfacial layer in $Hf_xZr_{1-x}O_2$ devices as opposed to the interfacial layer thickness effect. ZrO_2 devices have thicker interfacial layers than $Hf_xZr_{1-x}O_2$ devices; yet, they have greater mobility degradation. Thus, the observed mobility improvement cannot simply be due to differences in interfacial layer thicknesses in HfO_2, $Hf_xZr_{1-x}O_2$, or ZrO_2. All these data indicate that $Hf_xZr_{1-x}O_2$ devices with 50–60% Zr content give optimum performance and are promising candidates for SiO_2 replacement for future CMOS generations.

Conclusion

In summary, physical and electrical characteristics of $Hf_xZr_{1-x}O_2$ deposited using TEMAHf(Zr) and ozone have been investigated. $Hf_xZr_{1-x}O_2$ films have excellent thermal stability and remain smooth

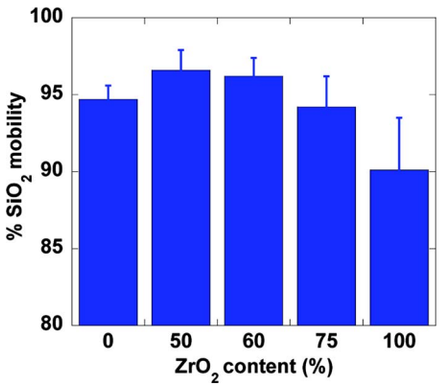

Figure 7. (Color online) Plot of percent SiO_2 high field mobility as function of Zr content for ~25 Å $Hf_xZr_{1-x}O_2$ (x = 0, 0.25, 0.4, 0.5, or 1) devices.

and void-free after high-temperature annealing. Stabilization of the tetragonal phase is observed with Zr addition. $Hf_xZr_{1-x}O_2$ devices exhibit lower threshold voltage and higher mobility than HfO_2 devices.

Freescale Semiconductor, Incorporated, assisted in meeting the publication costs of this article.

References

1. R. I. Hegde, D. H. Triyoso, P. J. Tobin, S. Kalpat, M. E. Ramon, H.-H. Tseng, J. K. Schaeffer, E. Luckowski, W. J. Taylor, C. C. Capasso, et al., *Tech. Dig. - Int. Electron Devices Meet.*, **2005**, 39.
2. W. J. Taylor, C. Capasso, B. Min, B. Winstead, E. Verret, K. Loiko, D. Gilmer, R. I. Hegde, J. Schaeffer, E. Luckowski, et al., *Tech. Dig. - Int. Electron Devices Meet.*, **2006**, 625.
3. D. H. Triyoso, R. I. Hegde, W. J. Taylor, Jr., R. Gregory, X.-D. Wang, J. K. Schaeffer, S. Filipiak, D. Gilmer, M. Raymond, K. Junker, et al., in *AVS Atomic Layer Deposition Conference Proceedings*, American Vacuum Society, p. 4 (2007).
4. R. I. Hegde, D. H. Triyoso, S. B. Samavedam, and B. E. White, Jr., *J. Appl. Phys.*, **101**, 074113 (2007).
5. M. Ritala and M. Leskela, in *Handbook of Thin Film Materials*, H. S. Nalwa, Editor, p. 103, Academic Press, San Diego, CA (2001).
6. R. Puurunen, *J. Appl. Phys.*, **97**, 121301 (2005).
7. P. D. Kirsch, M. A. Quevedo-Lopez, H. J. Li, Y. Senzaki, J. J. Peterson, S. C. Song, S. A. Krishnan, N. Moumen, J. Barnett, G. Bersuker, et al., *J. Appl. Phys.*, **99**, 023508 (2006).
8. D. H. Triyoso, R. I. Hegde, B. E. White, Jr., and P. J. Tobin, *J. Appl. Phys.*, **97**, 1 (2005).
9. Y. Senzaki, P. Seung, H. Chatham, L. Bartholomew, and W. Nieveen, *J. Vac. Sci. Technol. A*, **22**, 1175 (2004).
10. D. H. Triyoso, P. J. Tobin, B. E. White, Jr., R. Gregory, and X. D. Wang, *Appl. Phys. Lett.*, **89**, 132903 (2006).
11. J. K. Schaeffer, C. Capasso, R. Gregory, D. Gilmer, L. R. C. Fonseca, M. Raymond, C. Happ, M. Kottke, S. B. Samavedam, P. J. Tobin, et al., *J. Appl. Phys.*, **101**, 014503 (2007).
12. D. C. Gilmer, J. K. Schaeffer, W. J. Taylor, G. Spencer, D. H. Triyoso, M. Raymond, D. Roan, J. Smith, C. Capasso, R. I. Hegde, et al., in *Proceedings of the 36th European Solid-State Device Research Conference*, IEEE, p. 351 (2006).
13. J. Gallegos, III, D. H. Triyoso, and M. V. Raymond, *Microelectron. Eng.*, In press.
14. D. H. Triyoso, R. I. Hegde, J. K. Schaeffer, R. Gregory, X.-D. Wang, M. Canonico, D. Roan, E. A. Hebert, K. Kim, J. Jiang, et al., *J. Vac. Sci. Technol. B*, **25**, 845 (2007).